Chemical Engineering Journal 454 (2023) 139876

Contents lists available at ScienceDirect

Chemical Engineering Journal

journal homepage: www.elsevier.com/locate/cej

Fluorine substitution enabled superior performance of $Na_xMn_{2-x}O_{1.5}F_{0.5}$ (x = 1.05–1.3) type Na-rich cathode

Bala Krishnan Ganesan [a], Megala Moorthy [a], Ranjith Thangavel [b,*], Kyung-Wan Nam [c], Vanchiappan Aravindan [d,*], Yun-Sung Lee [a,*]

[a] School of Chemical Engineering, Chonnam National University, Gwangju 61186, Republic of Korea
[b] School of Energy Science and Engineering, Indian Institute of Technology Guwahati, Guwahati 781039, India
[c] Department of Energy and Materials Engineering, Dongguk University-Seoul, Seoul 04620, Republic of Korea
[d] Department of Chemistry, Indian Institute of Science Education and Research (IISER), Tirupati 517507, India

ARTICLE INFO

Keywords:
Fluorine substitution
Sodium-rich cathode
Oxygen loss
Sodium ion battery

ABSTRACT

Among the various sodium cathodes, the potential of Na-rich layered oxides is yet to be fully utilized. Unlike their Li counterparts, they are least explored and are at least a generation behind in development. Addressing the same, herein, Na-rich $Na_xMn_{2-x}O_{1.5}F_{0.5}$ ($x = 1.05–1.3$) type cathodes were synthesized successfully and analyzed as potential electrodes for Na-ion battery applications. Oxygen loss in Na-based transition metal oxides is a common issue, and it is effectively addressed by fluorine substitution. In contrast to exploring a particular stoichiometry as in other Na-deficient layered cathodes, herein, Na-content was gradually increased from 1.05 to 1.3. The cathodes were synthesized using a conventional solid-state approach and quenched to achieve high crystallinity. Compounds with different sodium stoichiometry were electrochemically tested in a half-cell configuration. Among these compounds, the $Na_{1.2}Mn_{0.8}O_{1.5}F_{0.5}$ electrode exhibited very high capacities of 178 and 122 $mAhg^{-1}$ at current densities of 10 and 1000 mA g^{-1}, respectively. The Na-rich $Na_{1.2}Mn_{0.8}O_{1.5}F_{0.5}$ cathode was systematically analyzed to understand the mechanism underlying its superior performance using various structural and electrochemical analyses. Furthermore, to demonstrate its practicality, the Na-rich $Na_{1.2}Mn_{0.8}O_{1.5}F_{0.5}$ cathode was coupled with a hard carbon and Na-In alloy anode in a full-cell assembly.

1. Introduction

Global warming is manifesting in various forms, such as the melting of ice in the poles and heavy rainfall and flash floods in European countries; several natural disasters may be linked to global warming, which primarily results from the increasing release of greenhouse gases such as CO_x and NO_x into the atmosphere. It is the people's responsibility to preserve mother nature. The transportation sector is one of the major contributors toward the emission of greenhouse gases. Hence, adopting a greener and more sustainable approach can lead to a greener planet for future generations. Contemporary fossil fuel-based modes of transportation should be phased out steadily and replaced by promising renewable alternatives such as electric, wind, or solar powers. However, this transition comes at a cost, which currently exceeds that of the existing fossil fuel systems, such as fuel cell technology and its battery packs. To overcome this issue, instead of relying on on-site energy generation, energy can be generated offsite (e.g., solar and wind farms) and transported via energy storage devices (e.g., batteries or supercapacitors). However, the prevalent innovative technology in energy storage, i.e., Li-ion batteries, are expensive and are severely plagued by supply chain disruptions, inadequate product development, and non-eco-friendly extraction methods. Na-ion batteries (NIB), however, are less expensive because sodium sources are abundant; however, the storage capacity of NIBs does not meet the exponentially increasing energy demand.

This issue may be addressed by increasing the capacity of the cathode. Ohsawa *et al.* [1] were one of the first groups to propose a cathode with surplus lithium in the transition metal (TM) layer. Although their work demonstrated a high initial charge/discharge in a high potential window of 4.5 V compared to that of Li/Li^+, their system suffered a cyclability issue due to the quantity of Li extracted and inserted during cycling. Later, Lu *et al.* [2,3] extensively studied Li-rich systems like $Li(Li_{0.2}Mn_{0.54}Ni_{0.13}Co_{0.13})O_2$ and reported that the formation of a mixed spinel-like layered structure after deep lithiation or de-lithiation was the

* Corresponding authors.
E-mail addresses: ranjith.t@iitg.ac.in (R. Thangavel), aravind.van@gmail.com (V. Aravindan), leeys@chonnam.ac.kr (Y.-S. Lee).

https://doi.org/10.1016/j.cej.2022.139876
Received 2 August 2022; Received in revised form 7 October 2022; Accepted 14 October 2022
Available online 27 October 2022

main cause for the capacity fade upon cycling. This could be partially addressed by surface modification using graphene to improve cyclability. However, this modification could only address the issue on a surface level, while the formation of the spinel-like structure is deeply rooted in the oxidation of oxygen at the lattice level, leading to irreversibility. Before Ohsawa *et al.* [1], Amine *et al.* [4] proposed Li$(Li_{0.2}Ni_{0.15+0.5z}Co_{0.10}Mn_{0.55-0.5z})O_{2-z}F_z$ with F-substitution primarily to suppress cell impedance and improve cyclability. Later, Fan *et al.* [5] substituted an F anion in the above stoichiometry and studied the improved electrochemical performance of the layered structures, since that by cation substitution was difficult to control owing to size differences. However, Lu *et al.* [6] reported that the F substitution both suppressed the cell impedance and also enlarged unit cell volume. Moreover, the F anion retarded the undesired spinel phase formation in the Li-rich layered structures. Various structural and surface modifications like $FePO_4$ coating [7] and various cation substitutions [8–11] have been reported recently. Ceder *et al.* [12,13] extensively studied such Li-rich cathodes, which evolve from layered to disordered rocksalt structures upon cycling. These studies opened up new opportunities for the scientific community to utilize materials with highly ordered and layered structure as high-performance cathodes [8,9,14–19]. Unlike the ordered structures wherein lithium 2D slabs and tetrahedral site 3D networks form structural support and enable higher capacity and cyclic stability, the disordered structures comprise random arrangements of Li and TM in the same sub-lattice that offer significantly better capacity and structural stability owing to a homogeneous distribution of cations [13].

As mentioned earlier, with the ever-increasing cost of lithium and its supply chain, the Li-rich system is irrational to solve the energy problem. Sodium is considered one of the best alternatives with the two key beats of NIB being, Na-deficient (Na < 1.0) layered [20–24] and Na-rich (Na > 2.0) cathodes like Prussian blue [25–30] and NASICON-type [31–34]. While the former has very less capacity compared to its Li-counterpart, the latter exhibits poor conductivity and stability for long-term usage. Hence, taking advantage of either system, a Na-rich cathode with a Na composition of 1.0–1.35 could fulfil the purpose of high capacity and superior performance. Much like their Li-counterparts, the Na-based cathodes are also affected by poor cyclability [35,36]. However, they have been least explored and are gaining traction only recently. Despite the widely prevalent problems of loss in cycle stability (due to spinel formation) and the corresponding structure collapse during cycling, very few attempts have been made to address the same. Similar to their Li-counterparts, very few studies regarding structural modification such as Na-substitution [24,37] and other cation modifications [36,38] have been reported. Furthermore, to the best of our knowledge, no studies have been reported on Na-rich cathode materials with anion modification, since fluorine substitution plays a key role in enhancing both capacity and stability, and is a low-cost straightforward enhancement made to the existing Na-based layered structure. Fluorine is important in increasing the oxidation potential in both electrodes and electrolytes, thereby improving their working potential and stability. For instance in NASICON type electrode such as $Na_3V_2(PO_4)_3$, F- was substituted and new robust analogues with improved capacity and stability were reported [39,40]. By increasing the substitution of fluorine in oxygen, the valency of TM can be decreased to a lower valent redox-active while keeping the excess-Na level fixed. Overall, the oxygen redox dependency is drastically reduced, leading to the mitigation of oxygen loss during cycling and a subsequent increase in capacity. The F-substitution also changes the voltage curve in the complex due to the modification in the redox behaviour of TM. Additionally, F tends to attract Na-ions in a sodium structure, leading to a Na-rich environment. Much like the "Li gettering effect," it must be plausible that the presence of F in a Na-rich environment makes F more strongly bonded to the remaining sodium during the charging process, and thus some portion of Na remains unextractable from the structure even at high voltages. In addition, to understanding the characteristics of $Na_xMn_{2-x}O_2$, i.e without fluorine substitution, we highly recommend to give a read on our earlier publication [41]. This previously reported material not only acting as background for this research but also gives better insight of non-fluorine substituted cathode and its performances. Comparing current result with this previous report can highlight the effect of F-substitution in an average performance cathode to superior performing cathode.

2. Experimental section

2.1. Materials synthesis

2.1.1. Synthesis of $Na_xMn_{2-x}O_{1.5}F_{0.5}$ (NMF)

NMF was synthesized via ball-milling and followed by thermal treatment, *i.e.*, a solid-state approach. Stoichiometric amounts of sodium carbonate (Sigma Aldrich, >99.5 %), manganese (III) oxide (Sigma Aldrich, 99 %), and sodium fluoride (Sigma Aldrich, 99 %) were milled thoroughly by ball milling using ethanol as a solvent. The resultant powder was dried, followed by the addition of 20 wt% citric acid (Sigma Aldrich, 99 %). The powder was pressed into pellets and heated to 700 °C for 12 h at a heating rate of 5 °C min^{-1} in a muffle furnace in an O_2 atmosphere. The resultant product was then quenched to room temperature in the vacuum atmosphere of the chamber of the glove box to yield NMF-1, NMF-2, NMF-3, and NMF-4 with sodium stoichiometry of Na1.05 ($x = 0.5$), Na1.1 ($x = 0.1$), Na1.2 ($x = 0.2$), and Na1.3 ($x = 0.3$), respectively. For comparison, NCM811 active material was purchased from Wellcoss Corporation Pvt. ltd. and used as received. For further studies, the samples were stored inside the glove box to avoid a direct contact with air and moisture.

2.2. Material characterization

The crystal structures were characterized by X-ray diffraction (XRD; Cu Kα radiation, Rint 1000, Rigaku, Japan) in the 2θ range of 10–80°. The lattice parameters were determined by Rietveld refinement using the Profex software [42]. The corresponding particle morphologies, elemental compositions, and internal structures were evaluated via field emission scanning electron microscopy (FE-SEM, S-4700, Hitachi, Japan) coupled with energy-dispersive X-ray spectroscopy (EDX) module and high-resolution transmission electron microscopy (HR-TEM; JEM-2000, EX-II, JEOL, Japan). The transition metal valency in the bulk of the sample was characterized via X-ray absorption spectroscopy (XAS measurement; R-XAS, Rigaku Japan) and analyzed using the Demeter software.

2.3. Electrochemical measurements

The electrochemical studies of all the samples were performed using CR2032 coin-cells assembled inside a glove box in a controlled atmosphere of ultra-pure argon. The cells comprised the synthesized material as the cathode and metallic Na as the anode, separated by a polypropylene separator, with 1 M $NaClO_4$ in a mixture of ethylene carbonate (EC) and diethyl carbonate (DEC) (1: 1, v/v) as the electrolyte. The electrode materials were prepared by mixing 280 mg of active material with 80 mg of carbon black and 40 mg of polyvinylidene difluoride (PVDF) binder dissolved in a known quantity of *N*-methyl-2-pyrrolidone (NMP) solvent. The obtained mixtures were coated on an aluminum current collector and dried in a vacuum oven at 160 °C for 4 h before cell fabrication. Galvanostatic charge–discharge (GCD) studies were performed for different voltage ranges at specific current rates varying from 0.01 to 1 A g^{-1}, using an Arbin BT-2000 battery testing system. Cyclic voltammetry and EIS analyses were conducted using an electrochemical analyzer (SP-150, Biologic, France).

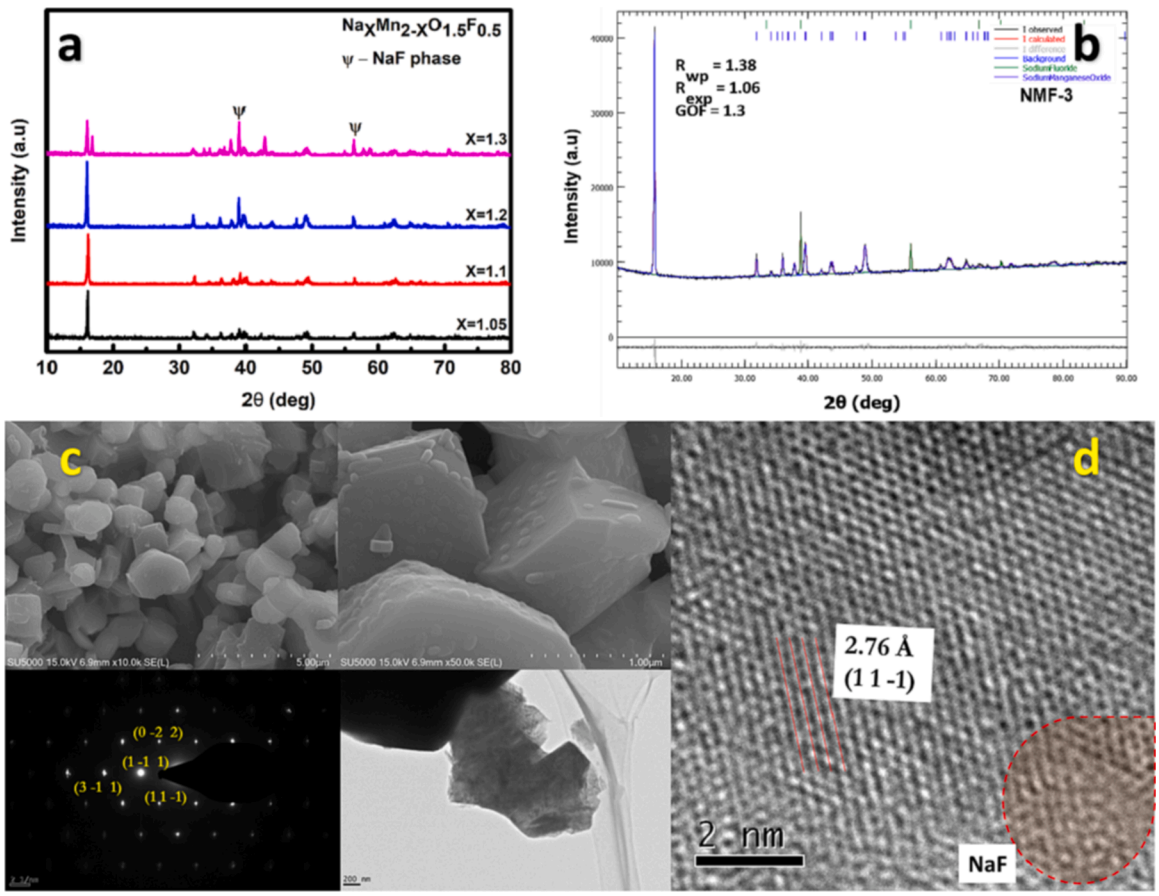

Fig. 1. (a) XRD images of Na-rich NMF materials with an increased sodium stoichiometry, (b) Rietveld analysis of NMF −3 cathode, and (c and d) SEM and TEM analyses of NMF-3 sample with the NaF disordered area highlighted by the red circle.

3. Result and discussions

3.1. X-ray diffraction analysis (XRD)

The initial structural characteristics of the newly developed NMF material were analyzed via XRD, as shown in Fig. 1a. Much like the layered Na-deficient cathodes, the Na-rich cathodes were also layered initially. However, unlike the layered oxide cathodes with doped anion wherein the crystal structures are not significantly affected, substituting the anion from O to F had a significant effect on the crystal structure of the $NaMnO_2$ layered structure, as shown in Fig. S1. Hence, to determine these structural and phase changes, XRD and its allied analysis techniques were extensively used. The sharp peaks of XRD indicated a highly ordered crystalline structure with the maximum peaks matching PDF card# 04–020-1862 of $NaMnO_2$ and PDF card#00–036-1455 of NaF. Based on the initial analysis, it was understood that the NMF material was composed of the aforesaid two phases co-existing. The high-intensity peaks of $NaMnO_2$ at 15.8° corresponding to the (0 0 2) plane and NaF at 33.47° corresponding to the (1 1 1) plane were a good match. Upon increasing the Na content from 1.05 to 1.3, the high-intensity peak at 15.8° shifted toward higher 2θ due to the tensile stress formation by a change in the lattice parameters.

3.2. Electron microscopy

To further understand the crystallinity and surface topography of the synthesized material, it was analyzed via electron microscopy, as shown in Fig. 1(c and d). FE-SEM previews the particle size and surface texture, whereas HR-TEM gives insights into the crystallinity and interlayer morphology of crystals. Hence, the $Na_{1.2}Mn_{0.8}O_{1.5}F_{0.5}$ cathode was analyzed using both FE-SEM and HR-TEM. In FE-SEM, the particle size was analyzed to be cubic and rhombohedral with a size of ~2 μm. Upon higher magnification, the surface was observed to be planar with small patches of carbon. Citric acid was used as a carbon source before the sintering process that may have left an uneven or patchy carbon coating around the solid particles. In HR-TEM, the high crystallinity of the sample was observed with evident interlayer fringes. The multi-planar structure of the cathode was evidently prominent, as shown in real space in Fig. 1d. Highly distinguishable spots in the selected area electron diffraction (SAED) pattern further confirmed the high order of crystallinity in the cathode.

3.3. Electrochemical studies

To evaluate the various electrochemical performances of the system, various electrochemical techniques such as cyclic voltammogram (CV), galvanostatic charge–discharge (GCD), and differential capacity profiles (dQ/dV) were utilized. In GCD, the electrochemical performance of the cathode material for energy storage was systematically analyzed. The electrochemical cell was cycled through current densities varying from 10 to 1000 mA g^{-1} to analyze its energy storage performance, as shown in Fig. 2. Unlike the usual cathode materials, which exhibit an initial charging capacity greater than their discharge counterpart, these materials exhibited greater discharge capacity than their charging counterpart due to a higher initial open-circuit voltage (OCV) and the upper cut-off potential capped at 4.0 V *vs* that in Na/Na^+. Also in the cycling profile of NMF-3, first charge capacity was about 89 mAh g^{-1}, which corresponds to 0.32Na^+ per formula unit. Thus in the first charge this composition act as limiting barrier displaying much lesser charging capacity. Upon subsequent discharge, the structure is recouped with

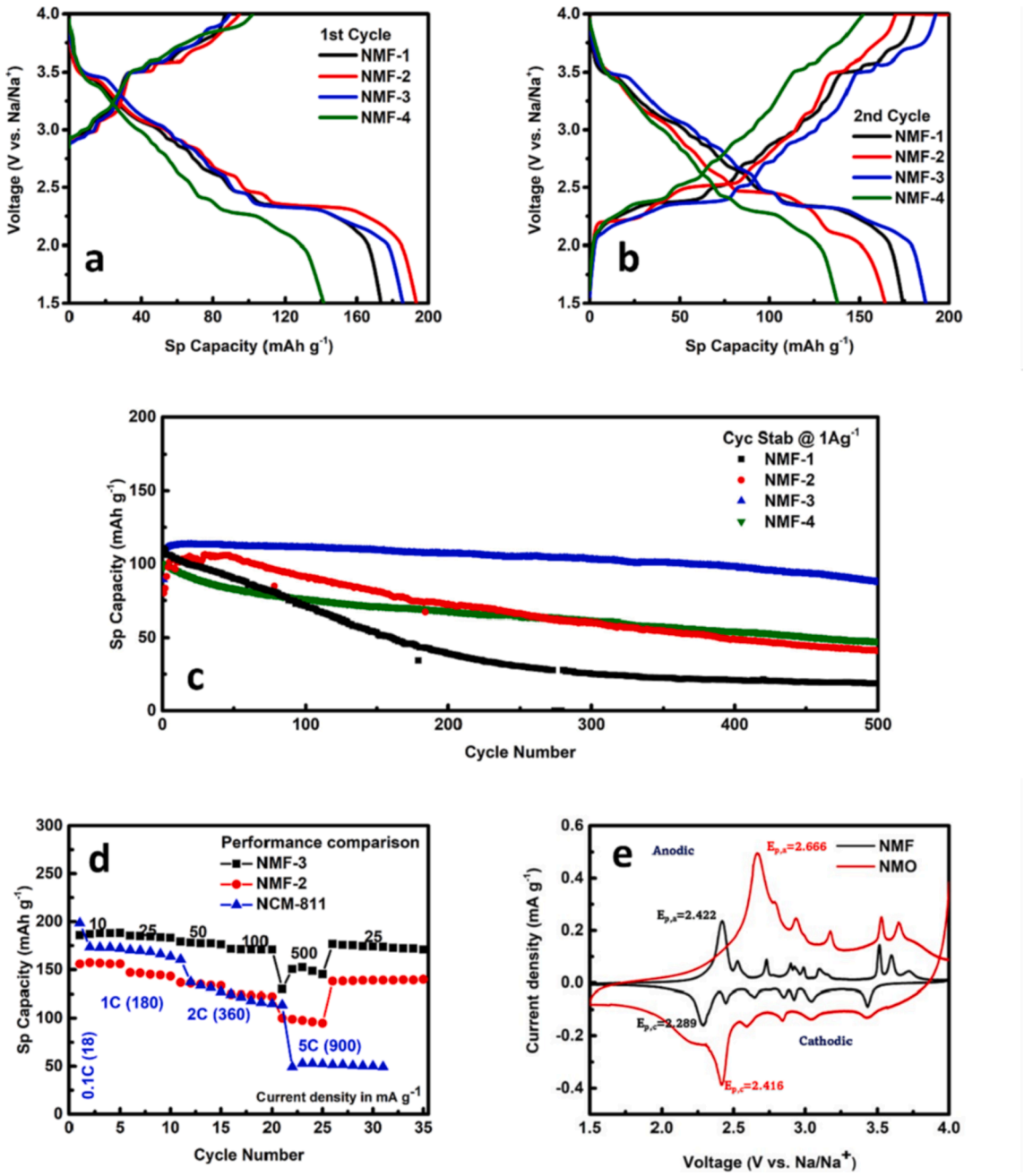

Fig. 2. (a and b) Galvanostatic charge–discharge curves of NMF samples for the 1st and 2nd cycle, (c) Cycle stability (discharge capacity) of NMF samples at a potential window of 1.5–4.0 V *vs* Na/Na^+ at a current density of 1 A g^{-1}, (d) rate performance of NMF samples at different current densities, and (e) cyclic voltammogram of $NaMnO_2$ and NMF-3 in the same potential window, normalized by current density.

sodium, which is removed in subsequent charge cycle normally and giving higher charging capacity. It is to be noted that GCD feature of NMF samples are very much in similar, multistep as in P2 $Na_{2/3}MnO_2$[43].The charge–discharge capacity became more balanced in the subsequent cycles owing to sufficient Na-ions shuttling from and to the cathode. Moreover, the redox reactions happened in a multi-step process due to the participation of the F anion. Upon increasing the current density to 10, 50, 500, and 1000 mA g^{-1}, the corresponding capacity drop was minimal at about 180, 169, 140, and 118 mAh g^{-1}, respectively. Such a performance of NMF-2 and 3 surpassed even that of the Li-NCM811 cells, as shown in Fig. 2. Overall, the F substitution had a great synergistic effect on the redox property of the Na-rich layered cathode material. To investigate this superior activity in depth, the cells were extensively analyzed via CV.

In the CV analysis, the reduction and oxidation processes of $Na_{1.2}Mn_{0.8}O_{1.5}F_{0.5}$ (NMF-3)were studied. Unlike a $NaMnO_2$ cathode, wherein Mn in the transition metal layer undergoes the redox process, herein the participation of an anion such as O and F was evident with the presence of multiple distinct redox peaks. To better understand this redox activity, the CV analysis was performed at a scan rate of 0.1 mV s^{-1}, helping to better capture every redox peak. As shown in Fig. 2e, the multi-electron transfer mechanism of $Na_{1.2}Mn_{0.8}O_{1.5}F_{0.5}$ is very similar to that of $NaMnO_2$ (NMO). Although the electroactive species remained the same, no additional redox peaks were observed; however the peak potentials were significantly altered. In NMF, the peaks were well separated and distinct, implying a step-by-step electron transfer, whereas NMO showed broader but fewer peaks of multiple electron transfer. The distinct appearance of the peak was attributed to the lower

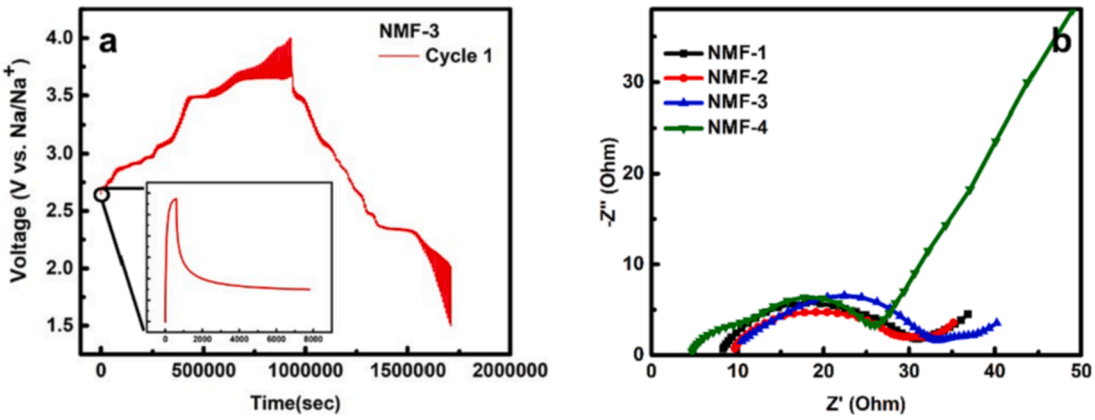

Fig. 3. (a) GITT curve of NMF-3 material with one step in an inset, and (b) electrochemical impedance spectra of NMF samples before cell testing.

electron transfer resistance or higher reversibility. The peak separation of the predominant redox peaks/polarization (ΔE_p) was determined by the reversibility of the electrode process. When ΔE_p was closer to ~57 mV, the process was highly reversible, and in the present case, ΔE_p of NMF was ~133 mV, while that of NMO was 249 mV, indicating the superior reversibility of the latter with less polarization.

To optimize the working potential window of the cathodes, the NMF sample was cycled in two different potential windows of 1.5–4.0 V *vs* Na/Na^+ and 2.0–4.5 V *vs* Na/Na^+, as shown in Fig. S2. Evidently, the electrode demonstrated better reversibility and cycle stability when worked between 1.5 and 4.0 V *vs* Na/Na^+. When the electrodes were pushed beyond 4.0 V *vs* Na/Na^+, a structural distortion potentially kicked in and a consistent fade in the peak currents was observed with each cycle. In Fig. S2, it can be noted that before the 1st cycle, the spike in current is observed for both the voltage windows due to oxygen loss, which was sufficiently suppressed in the subsequent cycles in the 4.0 V *vs* Na/Na^+ cycled sample, but remained unchanged when cycled at 4.5 V *vs* Na/Na^+ window. The initial oxygen loss was possibly due to the surface oxygen atoms, which were washed out in the 1st cycle, whereas the bulk of oxygen remained intact inside the structure. In addition to CV, the dQ/dV curve allowed for understanding and predicting the degradation and loss of capacity of NIBs. The differential capacity profile was proven to be a 'fingerprint' analysis to understand the underlying reaction kinetics and predict degradation upon cycling. In Fig. S3, the redox activity corresponding to the Mn^{3+} ion is observed to be significantly unleashed by the addition of an F^- anion, evident from the increasingly sharper peaks of Mn-redox in the potential range of 2.2–2.4 V *vs* Na/Na^+. In accordance with the Nernst equation, the reduction in applied potential (V) corresponded to the lesser effort needed to intercalate/de-intercalate Na from the electrolyte into the electrode surface, while its magnitude was given by the *y*-axis. Overall, it was evidently that the redox kinetics were significantly improved with F^- substitution.

3.3.1. *Diffusion studies*

The quantitative assessment of Na-diffusivity in various Na-rich structures was done via gravimetric intermittent titration technique (GITT) measurement with a relaxation time of 2 h after every charging or discharging increment. Overall, an optimal overpotential was observed, as illustrated in Fig. 3a. The Na-diffusion co-efficient was estimated to be in the range of 10^{-15}-10^{-11} cm^2 s^{-1} for NMF-3, better than that of most other sodium cathodes [44–46]. The unit cell volume was considered here for the calculation of diffusivity. It can be noted that the Li-diffusion co-efficient in layered $LiCoO_2$ is ~10^{-13}-10^{-11} cm^2 s^{-1}. Overall, the addition of fluorine significantly increased the Na-ion diffusivity, making it comparable to that of Li in Li-based layered cathodes. Electrochemical impedance spectra (EIS) is a powerful and non-destructive technique that utilizes AC signals to probe the impedance characteristics of an electrochemical system. Though it is very common for Na-rich cathode materials to have poor conductivity as seen in our earlier study on Na-rich oxide cathodes[41] in the NMF samples the F substitution significantly improved their electrical conductivity to ~20–30 Ω from hundreds of ohms (Fig. 3b). This increase in conductivity eventually helped improve the overall capacity of the Na-rich

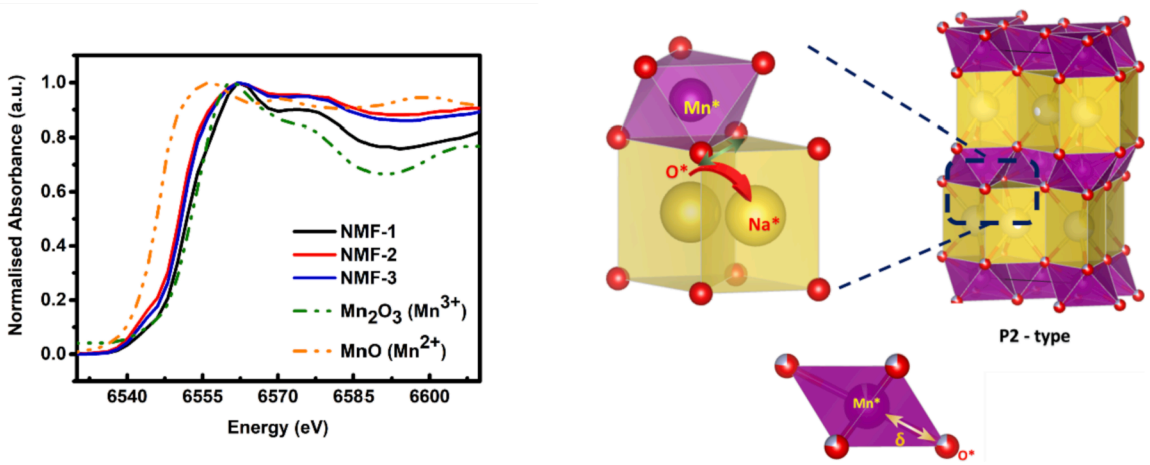

Fig. 4. (a) XANES spectra of NMF materials in comparison to Mn_2O_3 and MnO, (b) the schematic represents Na-diffusion in NMF crystal structure, whereas δ represents bonding distance between Mn* and O* atoms.

Table 1
Calculated cell parameter data using Rietveld refinement.

Sodium stoichiometry	Phase fraction		Cell parameters ($Na_xMnO_{1-y}F_y$)				R_{wp} (%)	R_{exp} (%)	χ^2	GOF
	$Na_xMnO_{1-y}F_y$	NaF	*a* (nm)	*b* (nm)	*c* (nm)	β(°)				
1.05	1.0	0.00	0.283 (±0.0005)	0.527 (±0.0007)	1.122 (±0.0002)	90.465 (±0.010)	1.71	1.14	2.25	1.5
1.1	0.8013	0.199	0.283 (±0.0002)	0.525 (±0.0002)	1.123 (±0.0002)	90.395 (±0.008)	1.37	1.1	1.55	1.25
1.2	0.754	0.256	0.283 (±0.0003)	0.524 (±0.0005)	1.122 (±0.0001)	90.271 (±0.007)	1.38	1.06	1.69	1.3
1.3	0.718	0.282	0.283 (±0.0001)	0.528 (±0.0001)	1.118 (±0.0003)	90.43 (±0.030)	2.5	1.06	5.61	2.37

cathodes upon the charge storage process [47].

3.4. X-ray absorption near-edge spectra analysis (XANES)

Although the chemical kinetics were significantly improved upon F-substitution, it remained unknown how the F-substitution enhanced the capacity and stability. Based on the CV studies with changes in the redox potentials of Mn, it was evident that the F anion somehow influenced the Mn cation. Based on the previous studies on Li-systems, it was understood that anion substitution could alter the TM valance state. Hence, to study the same in the current Na-based system, X-ray absorption near-edge spectra (XANES) were analyzed, as illustrated in Fig. 4a. XANES uses X-ray photons to study the inner core of a given atom and its valance state. On studying the spectra of the NMF samples in comparison with that of Mn_2O_3 and MnO for +3 and +2 oxidation states, a shift in the spectra towards Mn^{2+} was observed upon an increase in the Na content or decrease in the Mn content. This was contrary to the expectation that the valency of Mn increases from 3+ to 4+ with an increase in Na stoichiometry. The F anion played a crucial role in reducing the oxidation state of Mn^{3+} to Mn^{2+} To confirm this by linear combination fitting, the XANE spectra were fitted for all the samples, and the corresponding fitting results are presented in Table S1. With XANES, it was confirmed that the Mn cation valency was reduced, and hence an improvement in the NMF sample capacity was achieved.

3.5. Rietveld analysis

To further investigate the structural changes resulting from the increase in Na content or Mn oxidation state and its effect on the lattice parameters, Rietveld analysis was performed using the Profex software. Similar to the trends followed in its Li- counterparts[7], a parabolic change in the lattice parameter '*c*' value was observed. The increase in Na content followed a parabolic path for the peak value with a minima at Na-1.3, increasing further beyond. Among all the samples, the peak with the highest intensity was observed at Na-1.3 owing to its highly ordered structure. The changes in the structural parameters with increasing in Na content are tabulated in Table 1. Interestingly, with significant changes in the *b* and *c*-values of the crystal structure, the cell volume remained constant. This resulted from the changes in the *b* values being compensated by those in the *c* values. Upon the substitution of F for O, the cell volume remained the same due to their almost similar sizes. Unlike in the F-doped cathodes, an increasing trend of NaF was observed with decrease in Mn content or increase in Li content. It was suspected that F preferred Mn as the first choice to Na, and thus, Mn-rich NMF-1 had the least NaF phase. The F anion both preferred Mn to Na and altered its valency, as confirmed by the XANES analysis. Due to this change in Mn valency, the bond length of Mn* – O* marginally increased, leading to an increase in the size of the Na-layer facing the octahedra face. This further improved the Na-ion conductivity by providing a facile pathway and minimizing restrictions caused by the nearby TM layer. Overall, the F anion substitution preferred the Mn atom and altered its valency from +3 to near +2. Due to this change in valency, the bond length of Mn* – O* bond length δ increased from 2.139 (NMF-1) to 2.156 Å (NMF-3), leading to a less restricted diffusion path for Na-ion, as shown in Fig. 4b. Moreover, due to the change in the Mn-ion valency, additional Na could be accommodated, leading to an increased capacity, which was clearly evident from GCD.

3.6. In situ XRD analysis

To understand the mechanism behind the highly stable charge–discharge characteristics of the NMF-3 electrode, *in situ* XRD was performed, as presented in Fig. 5. The *in situ* mechanism was recorded using X-ray from a synchrotron source for reduced noise and higher accuracy. The cell was cycled at a current density of 10 mA g^{-1} between 1.5 and 4.0 V *vs* Na/Na^+ for the 1st charge–discharge and subsequent charge. Throughout this charge–discharge cycle, changes in the peaks of $NaMnO_2$ were observed, whereas those of NaF remained inactive throughout the process. Although the NaF phases were electrochemically inactive, they formed the basis of structural integrity and also an extra sodium reservoir for the sodium-depleting electrodes after cycling. Unlike LiF, which was both less conductive and electrochemically active, NaF was highly conductive, and thereby enhanced the Na-ion conductivity during cycling. It conformed well with the Rietveld data

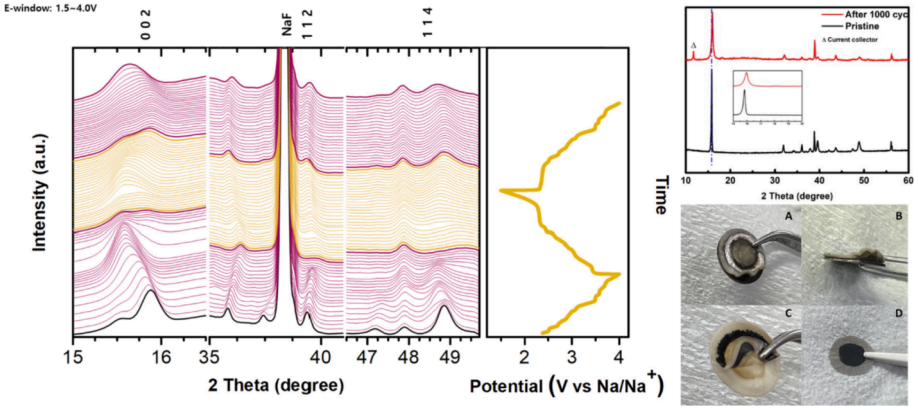

Fig. 5. In situ XRD spectra of NMF-3 sample cycled between E window of 1.5–4.0 V *vs* Na/Na^+ at a current density of 10 mA g^{-1} (left), post-mortem analysis of cell cycled for 1000 cycles (right), and XRD analysis (top). Images of (A and B) Na-anode, (C) separator, glass fiber, and (D) cathode mesh.

Table 2
Comparison on cathode performance with cation-rich electrodes.

Cathode reported by	Current density (mA g^{-1})	C-rate	Capacity (mAh/g)	Reference
Our work	1000		122	
Kim *et al.*	1600	25	65	[24]
Ho Ha *et al.*		0.5	90	[48]
Gupta *et al.*		0.05	100	[49]
Jian *et al.*	100		178	[45]
Song *et al.*		0.091	111.6	[50]
Lu *et al.*	300		94	[37]
Klee *et al.*		2	92	[31]
Song *et al.*		1	133	[35]
Song *et al.*	180	0.05	14.45	[51]
Shen *et al.*		0.5	86	[52]
Su *et al.*		2	111	[36]
Li *et al.*		5	70	[33]
Zhan *et al.*		0.5	112.2	[53]
Wu *et al.*		20	90	[32]

that with an increase in the NaF content, the stability increased, but with Mn, the capacity increased. Thus the right balance of both Mn and NaF contents was required to achieve both high capacity and stability $Na_xMn_{2-x}O_yF_{1-y}$ electrode. From the studies of the Li counterparts, it is well known that an adequate F content can suppress dendrite growth. To understand this, the electrodes were made using gum and cycled for 1000 cycles at a current density of 1000 mA g^{-1}. As shown Fig. S5, EIS data indicates the marginal increase in cell-resistance from 31 Ω to 57 Ω even after 1000 cycles indicating the superior stability of sample. Post-cycling, the cell was dismantled, and a post-mortem analysis was performed to study the structural integrity, wherein the capacity fade was found minimal even after 1000 cycles at a current density of 1 A g^{-1}. As shown in Fig. 5, the cathode remains intact even after 1000 cycles, as confirmed by XRD. However, the damage on the anode end was severe, and was significantly mitigated by the separator. Overall, the superior performance of cathode in comparison to earlier reports is given in Table 2

Lastly, to prove the applicability of this cathode for real-time application in a solid-state battery, NIBs were made with hard-carbon and a Na-In alloy as the anodes. As shown in Fig. S4, the metal-alloy NIB outperformed its hard-carbon-based counterpart due to the capacity limitations of hard carbon in the latter. Moreover, in terms of cycle stability, the hard-carbon-based cells exhibited poor cycle stability due to the consistent fading of the anodic side. Whereas, in the case of Na-In alloy, the capacity retention was ~94 % after 100 cycles. Overall, $Na_{1.2}MnO_{1.5}F_{0.5}$ display better performance than Li benchmark of NCM811 in terms of capacity and rate performance at higher current densities and cycle stability. Please note that operating voltage is lesser for sodium ion battery compared to Lithium and overall performance may be inferior to lithium. However this material can be considered as an important candidate for next generation of sodium cathode indicating a significant leap in reducing the cost of fast-charging NIBs for commercial use).

4. Conclusion

Recent trends suggest that industries are more focused on energy materials with superior cyclability at higher current rates for a faster charging process. To enhance cyclability, the structural integrity of the material is very important. Herein, the anion substitution of F for O both enhanced the capacity of the cathode by reducing the transition metal valency and significantly increased the cycle stability by reducing oxygen redox. In comparison, the capacity of the F substituted NMF-3 outperformed even that of NCM811 at a higher current rate for fast charging applications. In addition to analyzing the cathode performance, the effect of fluorine substitution in the cathode structure and transition metal valency were systematically studied and analyzed using Rietveld, *in situ*-XRD, and XANES. However, this paper studied only 25 % F-substitution (i.e., $O_{1.5}F_{0.5}$) at an anion site based on previous theoretical studies on the lithium counterparts. Hence, this study opens up new application opportunities for Na-rich cathode materials with F-substitution, wherein the various levels of F substitutions can be studied in the future.

Declaration of Competing Interest

The authors declare that they have no known competing financial interests or personal relationships that could have appeared to influence the work reported in this paper.

Data availability

Data will be made available on request.

Acknowledgements

This work was supported by the National Research Foundation of Korea (NRF, Korea) grant funded by the Korean government (Ministry of Science, ICT & Future Planning) (No.2019R1A2C1007620). Dr. Ranjith Thangavel acknowledges financial support from the Science & Engineering Research Board (SERB), a statutory body of the Department of Science & Technology (DST), Govt. of India, through the Start-up Research Grant (SRG/2022/000642). VA acknowledges financial support from the Science and Engineering Research Board (SERB), a statutory body of the Department of Science & Technology (DST), Govt. of India, for Swarna Jayanti Fellowship (SB/SJF/2020-21/12). BK would like to thank Ms Abinaya Sankaran, University of Limerick for constant support and discussions.

Appendix A. Supplementary data

Supplementary data to this article can be found online at https://doi.org/10.1016/j.cej.2022.139876.

References

[1] A. Ito, D. Li, Y. Sato, M. Arao, M. Watanabe, M. Hatano, H. Horie, Y. Ohsawa, Cyclic deterioration and its improvement for Li-rich layered cathode material Li $[Ni_{0.17}Li_{0.2}Co_{0.07}Mn_{0.56}]O_2$, J. Power Sources. 195 (2010) 567–573, https://doi.org/10.1016/J.JPOWSOUR.2009.07.052.
[2] B. Song, Z. Liu, M.O. Lai, L. Lu, Structural evolution and the capacity fade mechanism upon long-term cycling in Li-rich cathode material, Phys. Chem. Chem. Phys. 14 (2012) 12875–12883, https://doi.org/10.1039/C2CP42068F.
[3] B. Song, M.O. Lai, Z. Liu, H. Liu, L. Lu, Graphene-based surface modification on layered Li-rich cathode for high-performance Li-ion batteries, J. Mater. Chem. A 1 (2013) 9954–9965, https://doi.org/10.1039/C3TA11580A.
[4] S.H. Kang, K. Amine, Layered $Li(Li_{0.2}Ni_{0.15+0.5z}Co_{0.10}Mn_{0.55-0.5z})O_{2-z}F_z$ cathode materials for Li-ion secondary batteries, J. Power Sour. 146 (2005) 654–657, https://doi.org/10.1016/J.JPOWSOUR.2005.03.152.
[5] H. Li, L.Z. Fan, Effects of fluorine substitution on the electrochemical performance of layered Li-excess nickel manganese oxides cathode materials for lithium-ion batteries, Electrochim. Acta 113 (2013) 407–411, https://doi.org/10.1016/J.ELECTACTA.2013.09.135.
[6] L. Li, B.H. Song, Y.L. Chang, H. Xia, J.R. Yang, K.S. Lee, L. Lu, Retarded phase transition by fluorine doping in Li-rich layered $Li_{1.2}Mn_{0.54}Ni_{0.13}Co_{0.13}O_2$ cathode material, J. Power Sources. 283 (2015) 162–170, https://doi.org/10.1016/J.JPOWSOUR.2015.02.085.
[7] H. Zhang, T. Song, Synthesis and performance of fluorine substituted $Li_{1.05}(Ni_{0.5}Mn_{0.5})_{0.95}O_{2-x}F_x$ cathode materials modified by surface coating with $FePO_4$, Electrochim. Acta 114 (2013) 116–124, https://doi.org/10.1016/J.ELECTACTA.2013.10.030.
[8] Z. Lun, B. Ouyang, D.A. Kitchaev, R.J. Clément, J.K. Papp, M. Balasubramanian, Y. Tian, T. Lei, T. Shi, B.D. McCloskey, J. Lee, G. Ceder, Improved cycling performance of li-excess cation-disordered cathode materials upon fluorine substitution, Adv. Energy Mater. 9 (2019) 1802959, https://doi.org/10.1002/AENM.201802959.
[9] B. Ouyang, N. Artrith, Z. Lun, Z. Jadidi, D.A. Kitchaev, H. Ji, A. Urban, G. Ceder, Effect of fluorination on lithium transport and short-range order in disordered-rocksalt-type lithium-ion battery cathodes, Adv. Energy Mater. 10 (2020) 1903240, https://doi.org/10.1002/AENM.201903240.

[10] Y. Wang, H.T. Gu, J.H. Song, Z.H. Feng, X. Bin Zhou, Y.N. Zhou, K. Wang, J.Y. Xie, Suppressing Mn reduction of Li-Rich Mn-Based cathodes by F-doping for advanced lithium-ion batteries, J. Phys. Chem. C 122 (2018) 27836–27842, https://doi.org/10.1021/ACS.JPCC.8B08669/SUPPL_FILE/JP8B08669_SI_001.PDF.

[11] S. Chen, Y. Xie, W. Chen, J. Chen, W. Yang, H. Zou, Z. Lin, Enhanced electrochemical performance of Li-rich cathode materials by organic fluorine doping and spinel $Li_{1+x}Ni_yMn_{2-y}O_4$ coating, ACS Sustain. Chem. Eng. 8 (2020) 121–128, https://doi.org/10.1021/ACSSUSCHEMENG.9B04665/SUPPL_FILE/SC9B04665_SI_001.PDF.

[12] A. Urban, J. Lee, G. Ceder, A. Urban, J. Lee, G. Ceder, The configurational space of rocksalt-type oxides for high-capacity lithium battery electrodes, Adv. Energy Mater. 4 (2014) 1400478, https://doi.org/10.1002/AENM.201400478.

[13] J. Lee, A. Urban, X. Li, D. Su, G. Hautier, G. Ceder, Unlocking the potential of cation-disordered oxides for rechargeable lithium batteries, Science (80-.). 343 (2014) 519–522. 10.1126/SCIENCE.1246432/SUPPL_FILE/LEE.SM.PDF.

[14] Z. Cai, H. Ji, Y. Ha, J. Liu, D.-H. Kwon, Y. Zhang, A. Urban, E.E. Foley, R. Giovine, H. Kim, Z. Lun, T.-Y. Huang, G. Zeng, Y. Chen, J. Wang, B.D. McCloskey, M. Balasubramanian, R.J. Clément, W. Yang, G. Ceder, Realizing continuous cation order-to-disorder tuning in a class of high-energy spinel-type Li-ion cathodes, Matter 4 (2021) 3897–3916, https://doi.org/10.1016/J.MATT.2021.10.013.

[15] H. Ji, A. Urban, D.A. Kitchaev, D.H. Kwon, N. Artrith, C. Ophus, W. Huang, Z. Cai, T. Shi, J.C. Kim, H. Kim, G. Ceder, Hidden structural and chemical order controls lithium transport in cation-disordered oxides for rechargeable batteries, Nat. Commun. 2019 101. 10 (2019) 1–9. 10.1038/s41467-019-08490-w.

[16] D.A. Kitchaev, Z. Lun, W.D. Richards, H. Ji, R.J. Clément, M. Balasubramanian, D. H. Kwon, K. Dai, J.K. Papp, T. Lei, B.D. McCloskey, W. Yang, J. Lee, G. Ceder, Design principles for high transition metal capacity in disordered rocksalt Li-ion cathodes, Energy Environ. Sci. 11 (2018) 2159–2171, https://doi.org/10.1039/C8EE00816G.

[17] H. Ji, J. Wu, Z. Cai, J. Liu, D.H. Kwon, H. Kim, A. Urban, J.K. Papp, E. Foley, Y. Tian, M. Balasubramanian, H. Kim, R.J. Clément, B.D. McCloskey, W. Yang, G. Ceder, Ultrahigh power and energy density in partially ordered lithium-ion cathode materials, Nat. Energy 2020 53. 5 (2020) 213–221. 10.1038/s41560-020-0573-1.

[18] H. Ji, D.A. Kitchaev, Z. Lun, H. Kim, E. Foley, D.H. Kwon, Y. Tian, M. Balasubramanian, M. Bianchini, Z. Cai, R.J. Clément, J.C. Kim, G. Ceder, Computational investigation and experimental realization of disordered high-capacity li-ion cathodes based on ni redox, Chem. Mater. 31 (2019) 2431–2442, https://doi.org/10.1021/ACS.CHEMMATER.8B05096/SUPPL_FILE/CM8B05096_SI_001.PDF.

[19] Z. Lun, B. Ouyang, Z. Cai, R.J. Clément, D.H. Kwon, J. Huang, J.K. Papp, M. Balasubramanian, Y. Tian, B.D. McCloskey, H. Ji, H. Kim, D.A. Kitchaev, G. Ceder, Design principles for high-capacity mn-based cation-disordered rocksalt cathodes, Chemistry 6 (2020) 153–168, https://doi.org/10.1016/J.CHEMPR.2019.10.001.

[20] S. Guo, Y. Sun, J. Yi, K. Zhu, P. Liu, Y. Zhu, G.Z. Zhu, M. Chen, M. Ishida, H. Zhou, Understanding sodium-ion diffusion in layered P2 and P3 oxides via experiments and first-principles calculations: a bridge between crystal structure and electrochemical performance, NPG Asia Mater. 2016 84. 8 (2016) e266–e266. 10.1038/am.2016.53.

[21] C. Wang, L. Liu, S. Zhao, Y. Liu, Y. Yang, H. Yu, S. Lee, G.H. Lee, Y.M. Kang, R. Liu, F. Li, J. Chen, Tuning local chemistry of P2 layered-oxide cathode for high energy and long cycles of sodium-ion battery, Nat. Commun. 2021 121. 12 (2021) 1–9. 10.1038/s41467-021-22523-3.

[22] X. Chen, X. Zhou, M. Hu, J. Liang, D. Wu, J. Wei, Z. Zhou, Stable layered P3/P2 $Na_{0.66}Co_{0.5}Mn_{0.5}O_2$ cathode materials for sodium-ion batteries, J. Mater. Chem. A 3 (2015) 20708–20714, https://doi.org/10.1039/C5TA05205J.

[23] S. Komaba, C. Takei, T. Nakayama, A. Ogata, N. Yabuuchi, Electrochemical intercalation activity of layered $NaCrO_2$ vs. $LiCrO_2$, Electrochem. Commun. 12 (2010) 355–358, https://doi.org/10.1016/J.ELECOM.2009.12.033.

[24] D. Kim, S.H. Kang, M. Slater, S. Rood, J.T. Vaughey, N. Karan, M. Balasubramanian, C.S. Johnson, Enabling sodium batteries using lithium-substituted sodium layered transition metal oxide cathodes, Adv. Energy Mater. 1 (2011) 333–336, https://doi.org/10.1002/aenm.201000061.

[25] Y. Xi, Y. Lu, Rapid synthesis of sodium-rich prussian white for sodium-ion battery via a bottom-up approach, Chem. Eng. J. 405 (2021), 126688, https://doi.org/10.1016/J.CEJ.2020.126688.

[26] Z. Shen, S. Guo, C. Liu, Y. Sun, Z. Chen, J. Tu, S. Liu, J. Cheng, J. Xie, G. Cao, X. Zhao, Na-rich prussian white cathodes for long-life sodium-ion batteries, ACS Sustain. Chem. Eng. 6 (2018) 16121–16129, https://doi.org/10.1021/acssuschemeng.8b02758.

[27] X. Yan, Y. Yang, E. Liu, L. Sun, H. Wang, X.Z. Liao, Y. He, Z.F. Ma, Improved cycling performance of prussian blue cathode for sodium ion batteries by controlling operation voltage range, Electrochim. Acta 225 (2017) 235–242, https://doi.org/10.1016/j.electacta.2016.12.121.

[28] L. Wang, J. Song, R. Qiao, L.A. Wray, M.A. Hossain, Y. De Chuang, W. Yang, Y. Lu, D. Evans, J.J. Lee, S. Vail, X. Zhao, M. Nishijima, S. Kakimoto, J.B. Goodenough, Rhombohedral Prussian white as cathode for rechargeable sodium-ion batteries, J. Am. Chem. Soc. 137 (2015) 2548–2554, https://doi.org/10.1021/ja510347s.

[29] L.U. Subasinghe, G. Satyanarayana Reddy, A. Rudola, P. Balaya, Analysis of Heat generation and impedance characteristics of prussian blue analogue cathode-based 18650-type sodium-ion cells, J. Electrochem. Soc. 167 (2020), 110504, https://doi.org/10.1149/1945-7111/ab9ee9.

[30] R. Rehman, J. Peng, H. Yi, Y. Shen, J. Yin, C. Li, C. Fang, Q. Li, J. Han, Highly crystalline nickel hexacyanoferrate as a long-life cathode material for sodium-ion batteries, RSC Adv. 10 (2020) 27033–27041, https://doi.org/10.1039/D0RA03490H.

[31] R. Klee, P. Lavela, M.J. Aragón, R. Alcántara, J.L. Tirado, Enhanced high-rate performance of manganese substituted $Na_3V_2(PO_4)_3$/C as cathode for sodium-ion batteries, J. Power Sour. 313 (2016) 73–80, https://doi.org/10.1016/j.jpowsour.2016.02.066.

[32] T. Wu, J. Sun, Z.Q. Jeremy Yap, M. Ke, C.Y.H. Lim, L. Lu, Substantial doping engineering in $Na_3V_{2-x}Fe_x(PO_4)_3$ ($0 \leq x \leq 0.15$) as high-rate cathode for sodium-ion battery, Mater. Des. 186 (2020), 108287, https://doi.org/10.1016/j.matdes.2019.108287.

[33] H. Li, Z. Zhang, M. Xu, W. Bao, Y. Lai, K. Zhang, J. Li, Triclinic off-stoichiometric $Na_{3.12}Mn_{2.44}(P_2O_7)_2$/C cathode materials for high-energy/power sodium-ion batteries, ACS Appl. Mater. Interfaces 10 (2018) 24564–24572, https://doi.org/10.1021/acsami.8b07577.

[34] H.K. Roh, M.S. Kim, K.Y. Chung, M. Ulaganathan, V. Aravindan, S. Madhavi, K. C. Roh, K.B. Kim, A chemically bonded $NaTi_2(PO_4)_3$/rGO microsphere composite as a high-rate insertion anode for sodium-ion capacitors, J. Mater. Chem. A 5 (2017) 17506–17516, https://doi.org/10.1039/c7ta05252a.

[35] S. Song, M. Kotobuki, F. Zheng, Q. Li, C. Xu, Y. Wang, W.D.Z. Li, N. Hu, L. Lu, Na-rich layered $Na_2Ru_{0.95}Zr_{0.05}O_3$ cathode material for Na-ion batteries, J. Power Sources 342 (2017) 685–689, https://doi.org/10.1016/j.jpowsour.2016.12.116.

[36] N. Su, Y. Lyu, B. Guo, Electrochemical and in-situ X-ray diffraction studies of $Na_{1.2}Ni_{0.2}Mn_{0.2}Ru_{0.4}O_2$ as a cathode material for sodium-ion batteries, Electrochem. Commun. 87 (2018) 71–75, https://doi.org/10.1016/j.elecom.2017.12.029.

[37] Y. Lu, M. Yanilmaz, C. Chen, Y. Ge, M. Dirican, J. Zhu, Y. Li, X. Zhang, Lithium-substituted sodium layered transition metal oxide fibers as cathodes for sodium-ion batteries, Energy Storage Mater. 1 (2015) 74–81, https://doi.org/10.1016/j.ensm.2015.09.005.

[38] X. Zhang, Y. Qiao, S. Guo, K. Jiang, S. Xu, H. Xu, P. Wang, P. He, H. Zhou, Manganese-based na-rich materials boost anionic redox in high-performance layered cathodes for sodium-ion batteries, Adv. Mater. 31 (2019) 1807770, https://doi.org/10.1002/adma.201807770.

[39] L. Yue, C. Peng, C. Guo, X. Zhou, G. Li, N. Wang, J. Zhang, J. Liu, Z. Bai, X. Song Zhao, $Na_3V_{2-x}Fe_x(PO_4)_2O_2F$: an advanced cathode material with ultra-high stability for superior sodium storage, Chem. Eng. J. 441 (2022), 136132, https://doi.org/10.1016/J.CEJ.2022.136132.

[40] M. Wang, X. Huang, H. Wang, T. Zhou, H. Xie, Y. Ren, Synthesis and electrochemical performances of $Na_3V_2(PO_4)_2F_3$/C composites as cathode materials for sodium ion batteries, RSC Adv. 9 (2019) 30628–30636, https://doi.org/10.1039/C9RA05089B.

[41] B.K. Ganesan, U.R. Son, R. Thangavel, Y.-S. Lee, Effect of sodium addition on lattice structure and tuning performance in sodium rich $Na_xTm_{2-x}O_2$ type cathode materials (Tm=Mn and Cr; X=1.05–1.3) - a study, Electrochim. Acta 421 (2022), 140493, https://doi.org/10.1016/J.ELECTACTA.2022.140493.

[42] N. Doebelin, R. Kleeberg, Profex: a graphical user interface for the Rietveld refinement program BGMN, J. Appl. Crystallogr. 48 (2015) 1573–1580, https://doi.org/10.1107/S1600576715014685.

[43] D. Su, C. Wang, H.J. Ahn, G. Wang, Single crystalline $Na_{0.7}MnO_2$ nanoplates as cathode materials for sodium-ion batteries with enhanced performance, Chem. – A Eur. J. 19 (2013) 10884–10889, https://doi.org/10.1002/CHEM.201301563.

[44] L. Chen, S. Jin, H. Liu, S. Chen, Y. Dong, Q. Kuang, Y. Zhao, L. Chen, Structural and electrochemical studies of Fe-doped $Na_3Mn_2P_3O_{11}$ cathode materials for sodium-ion batteries, J. Alloys Compd. 821 (2020), 153206, https://doi.org/10.1016/j.jallcom.2019.153206.

[45] Z. Jian, H. Yu, H. Zhou, Designing high-capacity cathode materials for sodium-ion batteries, Electrochem. Commun. 34 (2013) 215–218, https://doi.org/10.1016/j.elecom.2013.06.017.

[46] W. Zuo, X. Liu, J. Qiu, D. Zhang, Z. Xiao, J. Xie, F. Ren, J. Wang, Y. Li, G.F. Ortiz, W. Wen, S. Wu, M.-S. Wang, R. Fu, Y. Yang, Engineering Na^+-layer spacings to stabilize Mn-based layered cathodes for sodium-ion batteries, Nat. Commun. 2021 121. 12 (2021) 1–11. 10.1038/s41467-021-25074-9.

[47] D.P. Siriwardena, J.F.S. Fernando, T. Wang, K.L. Firestein, C. Zhang, J.E. von Treifeldt, D.V. Golberg, Effect of Fe^{3+} for Ru^{4+} substitution in disordered $Na_{1.33}Ru_{0.67}O_2$ cathode for sodium-ion batteries: Structural and electrochemical characterizations, Electrochim. Acta 325 (2019), 134926, https://doi.org/10.1016/j.electacta.2019.134926.

[48] K.H. Ha, S.H. Woo, D. Mok, N.S. Choi, Y. Park, S.M. Oh, Y. Kim, J. Kim, J. Lee, L. F. Nazar, K.T. Lee, $Na_{4-\alpha}M_{2+\alpha/2}(P_2O_7)_2$ ($2/3 \leq \alpha \leq 7/8$, M = Fe, $Fe_{0.5}Mn_{0.5}$, Mn): a promising sodium ion cathode for na-ion batteries, Adv. Energy Mater. 3 (2013) 770–776, https://doi.org/10.1002/aenm.201200825.

[49] A. Gupta, C. Buddie Mullins, J.B. Goodenough, $Na_2Ni_2TeO_6$: evaluation as a cathode for sodium battery, J. Power Sources 243 (2013) 817–821, https://doi.org/10.1016/j.jpowsour.2013.06.073.

[50] W. Song, X. Ji, Z. Wu, Y. Yang, Z. Zhou, F. Li, Q. Chen, C.E. Banks, Exploration of ion migration mechanism and diffusion capability for $Na_3V_2(PO_4)_2F_3$ cathode utilized in rechargeable sodium-ion batteries, J. Power Sources 256 (2014) 258–263, https://doi.org/10.1016/j.jpowsour.2014.01.025.

[51] S. Song, M. Kotobuki, F. Zheng, C. Xu, N. Hu, L. Lu, Y. Wang, W.D. Li, Y-Doped Na_2ZrO_3: a Na-rich layered oxide as a high-capacity cathode material for sodium-

ion batteries, ACS Sustain. Chem. Eng. 5 (2017) 4785–4792, https://doi.org/10.1021/acssuschemeng.7b00196.

[52] B. Shen, M. Xu, Y. Niu, J. Han, S. Lu, J. Jiang, Y. Li, C. Dai, L. Hu, C. Li, Sodium-Rich Ferric Pyrophosphate Cathode for Stationary Room-Temperature Sodium-Ion Batteries, (2017). 10.1021/acsami.7b13516.

[53] R. Zhan, Y. Zhang, H. Chen, Q. Xu, Q. Ma, W. Gao, T. Yang, J. Jiang, S. Bao, M. Xu, High-rate and long-life sodium-ion batteries based on sponge-like three-dimensional porous na-rich ferric pyrophosphate cathode material, ACS Appl. Mater. Interfaces 11 (2019) 5107–5113, https://doi.org/10.1021/acsami.8b19874.